Larowska, D.; O'Brien, J. M.; Senge, M. O.; Burdzinski, G.; Marciniak, B.; Lewandowska-Andralojc, A. (2020): Graphene Oxide Functionalized with Cationic Porphyrins as Materials for the Photodegradation of Rhodamine B. The Journal of Physical Chemistry C 124, 15769−15780. doi: 10.1021/acs.jpcc.0c03907

Graphene Oxide Functionalized with Cationic Porphyrins as Materials for Photodegradation of Rhodamine B

Daria Larowska[1], Jessica M. O'Brien[2], Mathias O. Senge[2], Gotard Burdzinski[3], Bronisław Marciniak[1,4], Anna Lewandowska-Andralojc[1,4]*

[1]Faculty of Chemistry, Adam Mickiewicz University, Uniwersytetu Poznanskiego 8, 61-614 Poznan, Poland

[2] School of Chemistry, Trinity Biomedical Sciences Institute, Trinity College Dublin, The University of Dublin, 152-160 Pearse Street, Dublin 2, Ireland

[3]Faculty of Physics, Adam Mickiewicz University, Uniwersytetu Poznanskiego 2, 61-614 Poznan

[4]Center for Advanced Technology, Adam Mickiewicz University, Uniwersytetu Poznanskiego 10, 61-614 Poznan, Poland

alewand@amu.edu.pl

Abstract

Two non-covalent nanohybrids between cationic porphyrin (free base TMPyP and zinc(II) ZnTMPyP) bearing cationic (*N*-methylpyridyl) groups and graphene oxide (GO) were constructed with the aim of generating a photocatalyst active for Rhodamine B (RhB) degradation. The obtained materials were thoroughly characterized by steady-state and time-resolved absorption and emission methods which indicated that metalation of the porphyrin with Zn(II) increases the affinity of the porphyrin towards the GO surface. Photocurrent experiment together with femtosecond transient absorption spectroscopy clearly showed the existence of electron transfer from the photoexcited porphyrin to GO. Both hybrid materials demonstrated higher photocatalytic activity towards Rhodamine B degradation as compared to GO, however ZnTMPyP-GO exhibited more efficient performance (19% of RhB decomposition after 2 h of irradiation). Our data indicates that the presence of Zn(II) in the core of the porphyrin can promote charge separation in the ZnTMPyP-GO composites. The higher degradation rate seen with ZnTMPyP-GO as compared to the TMPyP-GO assemblies highlights the beneficial role of Zn(II)-metalation of the porphyrin ring.

Introduction

Organic heterocyclic dyes have wide industrial applications. They are commonly used in the textile, rubber, paper, plastic and cosmetic industries, and they are also well-known fluorescent water tracers.[1] Every day, a large amount of dyes is discharged into water as waste products, causing its contamination. Consequently, organic dyes are one of the most significant pollutants in wastewater due to their high toxicity and non-biodegradability in the environment. Some of them, such as Rhodamine 6G or Rhodamine B (Figure 1), have been reported to possess carcinogenic and mutagenic effects on living organisms.[2] Rhodamine B (RhB) is harmful to animals as it can cause irritation of the skin, eyes and respiratory tract.[3] Thus, taking into account its hazardous nature, it is worthwhile to make systematic efforts to degrade RhB from aqueous media.

Stability of the aromatic structure of dyes hinders their degradation using traditional methods such as biological and chemical oxidation. Although the adsorption technique using e.g. activated carbon is facile and efficient for the disposal of dyes, it involves expensive regeneration and disposing of huge amount of waste.[4,5] An ideal technique to efficiently remove organic dyes from waste water seems to be through a photocatalytic process, which has been eagerly pursued by scientists for decades.[6] In the last years notable progress has been made in increasing the efficiency of the photocatalysts, but still a number of issues needs to be improved such as more profound use of visible solar light, charge carrier recombination, stability of the photocatalysts and better control of the product selectivity. The most commonly used photocatalysts for dye degradation are inorganic semiconductor nanostructures *i.e.*, titanium dioxide,[7–9] zinc oxide,[10] or copper(II) oxide.[9] However, these photocatalysts can operate only under UV light irradiation. With efficient energy utilization in mind, research concentrated on the development of photocatalysts that function also

in visible range should be pursued eagerly.[11,12] In the solar spectrum visible light makes up as much as 47% which should be applied in the degradation of dyes and organic pollutants.[13]

Porphyrins, because of their intense absorption in the visible region, are frequently applicable in both natural and synthetic systems.[14] However, their hydrophobicity, the low photo-stability of the porphyrins themselves, as well as the presence of strong π-π interactions between the rigid macrocyclic molecules leads to aggregation which significantly diminishes practical applications.[15,16] By introducing the porphyrin structure to a support surface, the decrease of the photocatalytic activity caused by these strong π-π attractions between porphyrin molecules can be limited.

Outstanding properties of the graphene including good optical transmittance, large specific surface area, and conjugated aromatic system have made this material an ideal candidate for application as charge carriers or promoters.[17–20] However, as graphene has low solubility in aqueous media, its hydrophilic derivative graphene oxide (GO), can form stable aqueous suspensions which make it more suitable for direct use in the photodegradation of dyes from water. Up to now, several groups have reported on improved photocatalytic activity of porphyrin/graphene nanohybrids.[21–27] Due to the unique properties of GO and porphyrins, hybrid materials that combine both units were reported to be active in photocatalytic reactions[22] and solar energy conversion materrials.[28] In one report, Chen *et al.* employed vacuum filtration methods to prepare free standing films composed of *p*-THPP (tetrakis(*p*-hydroxyphenyl)porphyrin) nanoparticles and reduced graphene oxide (RGO) that showed enhanced photocatalytic activity for the degradation of organic pollutants (RhB and methyl blue) under visible light.[22] In another study, Guo *et al.* reported visible-light RhB photocatalytic degradation activity of a ZnTPyP

[(5,10,15,20-tetrakis(4-pyridyl)porphyrinato)zinc(II)] one-dimensional supramolecular nano-assembly formed *via* self-assembly assisted by GO.[21]

Herein, the non-covalent nanohybrids of two cationic porphyrins with GO are synthesized and characterized in view of their spectroscopic properties and applications in photodegradation of Rhodamine B (Figure 1). GO sheets, due to presence of oxygen-containing functional groups, possess negative charge in aqueous solutions under neutral pH, thus it is believed that both electrostatic attraction and π-π interactions will increase the affinity of the cationic porphyrin derivatives to the GO surface. In our previous studies it has been shown that electrostatic interactions between cationic 5,10,15,20-tetra(4-trimethylammoniophenyl)porphyrin tetra(*p*-toluenesulfonate) (TMAP) and negatively charged GO led to a strong interaction between the components and favored formation of the hybrid material with a higher content of the photoactive component.[29] It has been also demonstrated that ultrafast electron transfer and formation of the charge separated state occur between TMAP and GO,[29] which is crucial for efficient photocatalysts composed of graphene-type materials.

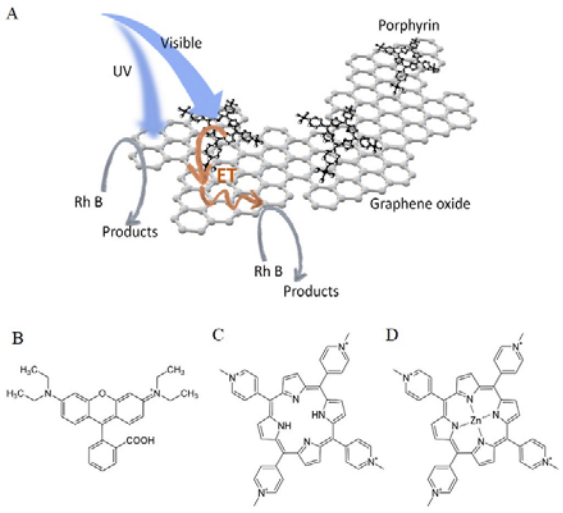

Figure 1. A) Scheme of RhB photodegradation in the system containing non-covalent porphyrin-GO hybrid, chemical structures of B) Rhodamine B, C) TMPyP and D) ZnTMPyP.

Significant interest among the scientific community in the construction of porphyrin- and graphene-based hybrids materials for photocatalysis resulted in number of reports.[16,21,24,26,27,30–36] However, the novelty of this study is the comprehensive comparison of spectroscopic properties between two hybrid materials composed of two water soluble porphyrins either free base or Zn(II) porphyrins bearing cationic (*N*-methylpyridyl) groups and GO and an analysis of how the difference in those properties affects photocatalytic activity towards RhB degradation. We have chosen a zinc porphyrin derivative because of the growing interest in using metalated porphyrins in photocatalytic processes.[23,27,37–39]

We are aware of only one study in which a comparison of the photocatalytic activity towards methylene blue (MB) of graphene porphyrin polymer nanocomposites prepared from different porphyrin monomers (free or zinc complexed) is given.[23] Interestingly the authors observed *ca.* 20 times lower activity for MB degradation for the nanocomposite containing a Zn(II)-porphyrin polymer. This significantly lower activity in comparison to corresponding free base porphyrin polymer/graphene composites was attributed to the monomer remaining in the sample as well as the lower efficiency of polymerization of the Zn(II)-porphyrin monomer. In our work we have focused on the changes in the spectroscopic properties of the monomer porphyrin-GO hybrid material upon metalation of the porphyrin core with Zn(II), and how these differences might be reflected in the photocatalytic performance of the hybrid material. It is shown that ZnTMPyP-GO exhibits higher efficiency for the photocatalytic degradation of RhB, which is most likely attributed to the longer-lived charge separated state.

1. EXPERIMENTAL

1.1 Reagents and materials

Graphene oxide was purchased from Abalonyx, Rhodamine B from Acros Organics, Anhydrous DMF from Sigma Aldrich and 2% colloidal solution of SnO_2 from Alfa Chemicals. Reagents for porphyrin syntheses were obtained from commercial sources and were used as received. Only pyrrole was first filtered through a plug of silica before use. All air- and/or water-sensitive materials were handled using standard high vac. procedures. For solution preparation millipore distilled water was used. The synthesis of TMPyP and ZnTMPyP is described in the Supporting Information along with ^{1}H NMR and MALDI spectra (Figures S1–S8).

1.2 Experimental apparatus

Absorption spectra were measured at room temperature on either a Jasco V-670 or a Specord 250 spectrophotometer in the range from 200-800 nm. Fluorescence spectra were recorded in the range of 500 and 800 nm on a LS 50B spectrofluorometer (Perkin Elmer) for the solutions with the absorbance at the excitation wavelength lower than 0.1. The florescence lifetimes were measured on a Fluorescence Lifetime Spectrometer (FluoTime300 from PicoQuant) with a detection system based on time-correlated single-photon counting (TCSPC). The emission decay lifetimes were measured following excitation with 440 nm photodiodes. Samples were placed in 10 mm quartz cells for all of the steady-state and time-resolved emission measurements. Photocurrent experiments were performed using a Keithley model 617 programmable electrometer probe station with a Fiber optic illuminator (Fiber-Lite®, Model 190). The details of the femtosecond transient absorption spectroscopy setup have been described elsewhere.[25] For transient UV-vis measurements a quartz cell with 2 mm optical path of solution was used with the absorbance of about 0.2 at the excitation wavelength. The sample solution was stirred by a Teflon-

coated bar. Typical pump energy was about 1 μJ. All experiments were performed at room temperature. Analysis of the transient absorption data was made using Surface Explorer software (Ultrafast Systems). NMR spectroscopy was carried out on a Brucker DPX 400 (400 MHz for ^{1}H NMR) spectrometer at room temperature using an appropriate deuterated solvent. Mass spectrometry results (HRMS) were obtained using a Q-Tof Premier Waters MALDI quadrupole time-of-flight (Q-TOF) mass spectrometer equipped with a Z-spray electrospray ionization (ESI) and a matrix assisted laser desorption ionization (MALDI) sources in positive mode with trans-2-[3-(4-*tert*-butylphenyl)-2-methyl-2-propenylidene]malononitrile as the internal matrix. A Digital Stuart SMP10 melting point apparatus was used to determine all melting points, which are uncorrected. Atomic force microscopy images were recorded on an AFM Agilent 5500 instrument. The samples for the AFM measurements were prepared by dropping diluted aqueous suspensions onto a mica surface and drying in air.

1.3 Photoelectrochemical measurements

Photoelectrochemical activities were measured on an electrochemical workstation (Keithley model 617 programmable electrometer) using a 0.1 M LiI acetonitrile solution as the electrolyte. Experiments were performed using a three-electrode configuration quartz cell. The platinum electrode was the counter electrode, a saturated calomel electrode (SCE) was used as the reference electrode, and GO-SnO_2-FTO, TMPyP-GO-SnO_2-FTO or ZnTMPyP-GO-SnO_2-FTO electrodes acted as the working electrodes. Photocurrents of the working electrodes with and without irradiation were measured at 0 V using a Fiber optic illuminator as the light source.

The preparation method of the working electrodes was as follows: a layer of SnO_2 was put on a fluorine-doped tin oxide (FTO) glass electrode *via* a doctor blading method and received thermal

treatment under an air atmosphere. The prepared samples were covered with graphene oxide *via* electrophoretic deposition. GO-SnO_2-FTO electrodes were left overnight in porphyrin baths (60 μM) and dried in air to achieve porphyrin functionalization on their surface.

1.4 Determination of the photocatalytic activity toward RhB degradation

Experiments of the RhB dye photodegradation were carried out in water at pH 6.5 containing the appropriate samples at ambient temperature. 3.448 mL of the aqueous catalyst samples (TMPyP-GO (0.42 mg, TMPyP 3.7% wt), ZnTMPyP-GO (0.41 mg, ZnTMPyP 4.9%), GO (0.4 mg)) were placed in a beaker (25 mL) and mixed with 8.34 mL of RhB (5 mg mL^{-1}) solution and 13.212 mL of H_2O. The mixture was stirred in the dark until it reached an adsorption-desorption equilibrium, after which 3 mL of the solutions were placed in a quartz cuvette and irradiated using a halogen lamp light source (150 W with a cut-off filter $\lambda > 400$ nm). Decrease of the RhB concentration was measured spectrophotometrically at 554 nm. The photocatalytic tests were repeated three times for each sample.

2. RESULTS AND DISCUSSION

Steady state absorption measurements

The absorption spectra of TMPyP and ZnTMPyP exhibited characteristic bands expected for porphyrins, *i.e.*, the Soret and Q-bands which are described by the Gouterman four-electron, four orbital model.[40,41] As shown in Figure 2, the UV-vis spectrum of TMPyP has an intense Soret band with the maximum at *ca.* 422 nm ($\varepsilon_{422} = 2.0 \times 10^5$ M^{-1} cm^{-1})[42] and four weaker Q-bands at *ca.* 518, 555, 584 and 643 nm. The insertion of Zn(II) into the porphyrin ring caused a red-shift of the Soret band by 15 nm together with the decrease of the molar absorption coefficient ($\varepsilon_{437} = 1.2 \times 10^5$ M^{-1} cm^{-1}). This red-shift of the Soret band can be explained by the fact that the zinc metalloporphyrin contains a closed-shell ion, in which zinc-based orbitals have low energy, and the energy gap

between the HOMO and LUMO of the porphyrin ring was reduced.[43] The UV-vis spectrum of ZnTMPyP is also characterized by two Q-bands at 566 nm and 613 nm. The decrease in the number of Q-bands in the UV-vis spectra of ZnTMPyP in comparison to TMPyP is attributed to the increase in the symmetry of the porphyrin ring upon metalation.[40,41]

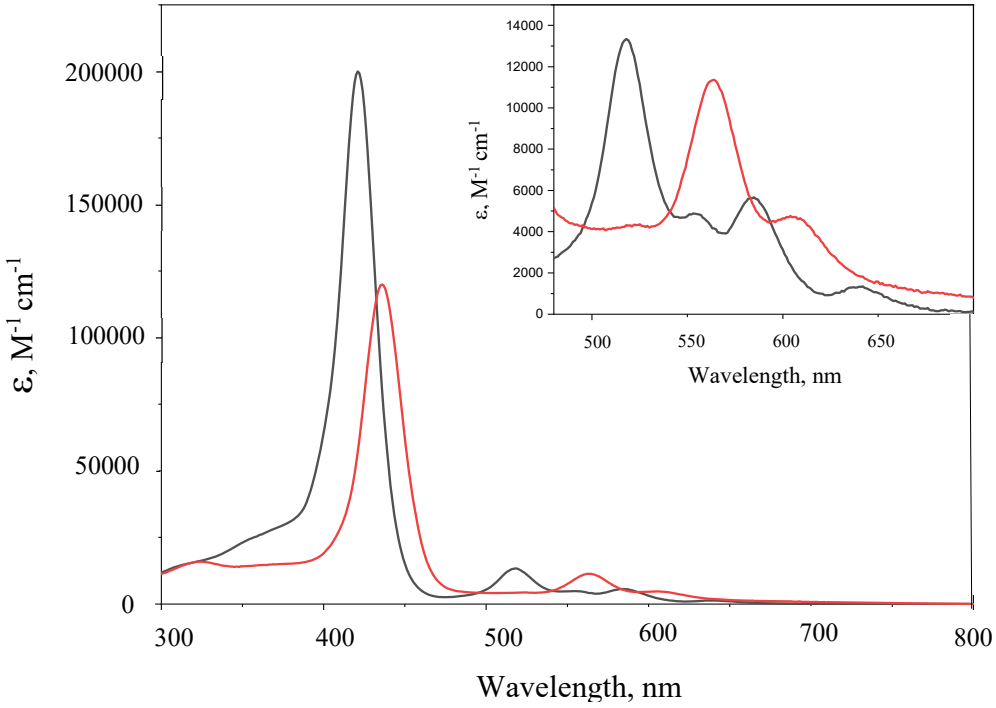

Figure 2 Absorption spectra of TMPyP (black) and ZnTMPyP (red) in water (inset: Q-band region of the same spectra).

Ground state interactions between GO and the porphyrins (TMPyP or ZnTMPyP) were probed by UV-vis spectroscopy. Figure 3A illustrates the optical absorption spectra of a series of solutions, in which GO was gradually added to an aqueous solution of TMPyP. The UV-vis spectra of the TMPyP changed significantly upon addition of GO. It can be noticed that the decrease of the absorbance at 422 nm is accompanied by a new band arising with a maximum at 440 nm (Figure

S9). These changes are attributed to the decrease of the concentration of free TMPyP together with the increase of the concentration of porphyrin bound to GO. The absorbance at 440 nm increased linearly with the added amount of GO dispersion and reached a maximum for the concentration of GO as low as 6.7×10^{-3} mg mL^{-1} (Figure S9). In addition, the presence of an isosbestic point at 434 nm indicates that there was clear change from free TMPyP to TMPyP adsorbed on GO surface. Figure 3B shows the UV-Vis spectra recorded during the addition of an aqueous suspension of GO to a 1.0 μM aqueous ZnTMPyP solution. A batochromic shift of the Soret bands position by 16 nm was detected together with the appearance of an isosbestic point at 447 nm. Notably, the extinction coefficients of the Soret bands of both porphyrins adsorbed to GO were lower than those of the free molecules (Table S1). The bathochromic shifts observed upon nanohybrid formation for both porphyrins could be explained by at least two different mechanisms: 1) J-aggregation of the porphyrin molecules, 2) flattening of the porphyrin molecule. The first possibility is highly unlikely since under our experimental conditions (pH 6.2) the porphyrin exists as a free base, bearing four positive charges at the *meso* substituents $–N(Me)_3^+$. Therefore, due to Columbic repulsion among the porphyrin molecules aggregation is not likely.[44] The clear isosbestic point observed during titration as well as the linear dependence of the absorbance at the maximum of the Soret band of nanohybrid on GO concentration (Figures S9) suggest that the obtained material has a well-defined structure. Also, only a slight broadening of the Soret band was observed for the adsorbed porphyrin. Moreover, the AFM images also provided solid evidence for the molecular assembly of cationic porphyrins on GO sheets. As shown in Figure S10, for non-functionalized GO in neutral aqueous suspension individual sheets of 1-2 μm lateral sizes were detected. The GO existed as a single sheet with the apparent thickness of ca. 0.9 nm.[45] On the depth profiles obtained for TMPyP-GO and ZnTMPyP-GO (Figure S10) the single layer GO together with additional

height jumps of c.a. 1 nm are detected. Considering that TMPyP and ZnTMPyP constitutes only 5 % and 9.9% weight of composites, respectively it is reasonable to assume that they do not cover whole GO surface. Assuming that the thickness of one porphyrin molecule is similar to the thickness of GO sheet we concluded that porphyrins molecules were adsorbed on GO sheets as single molecules, not aggregates.

A plausible reason for the observed red-shifts of the Soret bands in TMPyP-GO and ZnTMPyP-GO nanohybrids is the flattening of the porphyrin molecule when it is adsorbed on the GO surface. This explanation was discussed earlier for nanohybrids of TMPyP and RGO or chemically converted graphene (CCG) and TPPH or ZnTPPH with GO .[38,42,46,47] Theoretical calculations predict that only a 30° change in the orientation of the meso-substituents toward the porphyrin core can result in a batochromic shift of the Soret band by as much as 30 nm.[48] Our previous calculations have shown that the interaction of ZnTPPH and TPPH with graphene oxide leads to a twisting of the side rings relative to the porphyrin core from about 60° to 45° and 39° for ZnTPPH and TPPH, respectively,[38,47] confirming the flattening of the porphyrin upon complexation. Moreover, the experimentally observed Soret band red-shift of 16 nm for the ZnTPPH adsorbed on the GO surface was well reproduced in theory.[38] The slightly smaller red-shift observed for ZnTMPyP in comparison to TMPyP upon adsorption on GO (Figure S11) can be attributed to less profound flattening of the ZnTMPyP as observed previously for the TPPH and ZnTPPH.[38,47]

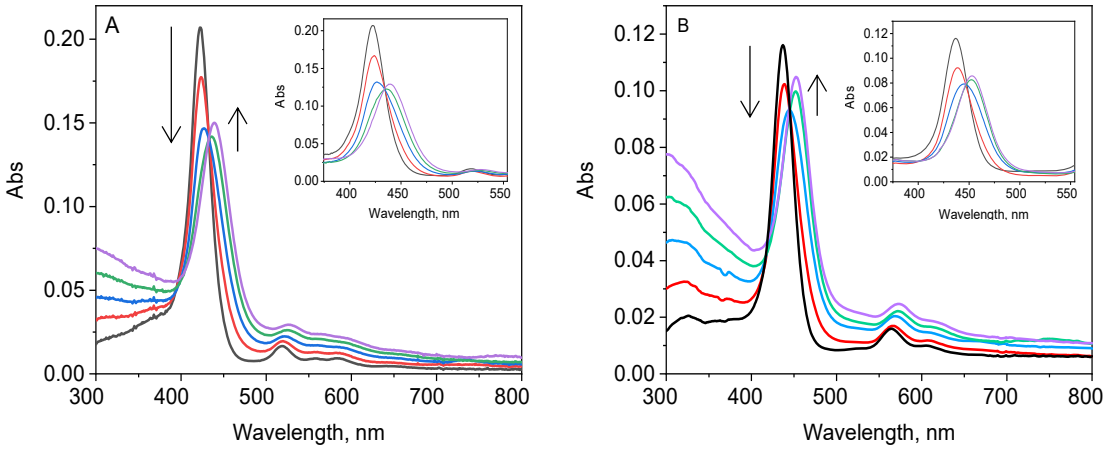

Figure 3 A) Absorption spectra recorded during addition of different amounts of an aqueous solution of GO (0 – 6.67 × 10^{-3} mg mL^{-1}) to a 1.0 μM aqueous TMPyP solution (inset: the same spectra corrected for the GO absorption); B) Absorption spectra recorded during the addition of different amounts of an aqueous solution of GO (0 – 6.67 × 10^{-3} mg mL^{-1}) to a 1.0 μM aqueous ZnTMPyP solution (inset: the same spectra corrected for the GO absorption); black – 0 mg mL^{-1}; red – 1.67 × 10^{-3} mg mL^{-1}; blue – 3.33 × 10^{-3} mg mL^{-1}; green – 4.99 × 10^{-3} mg mL^{-1}; purple – 6.67 × 10^{-3} mg mL^{-1};

Spectroscopic results clearly demonstrated that the interaction between GO and both porphyrins was profound already in the ground state and that the fabrication of the new hybrid materials is facile and is limited to the combining of two solutions containing porphyrin and GO. The possibility of isolation of the newly prepared porphyrin-GO materials was examined by a centrifugation experiment controlled by absorption spectroscopy. Figure 4 presents the UV-vis spectra of the suspension of the nanohybrids TMPyP-GO and ZnTMPyP-GO before and after centrifugation. Based on the minor peak attributed to the porphyrin in the UV-vis of the supernatant in both cases nearly the entire amount of the obtained nanohybrids was successfully

collected as a precipitate. A strong interaction of the porphyrins with GO can be explained by the Coulombic attraction between cationic TMPyP and ZnTMPyP and GO that possesses a negative charge (pK_a of the carboxyl group in GO was reported to be 4.3).[49]

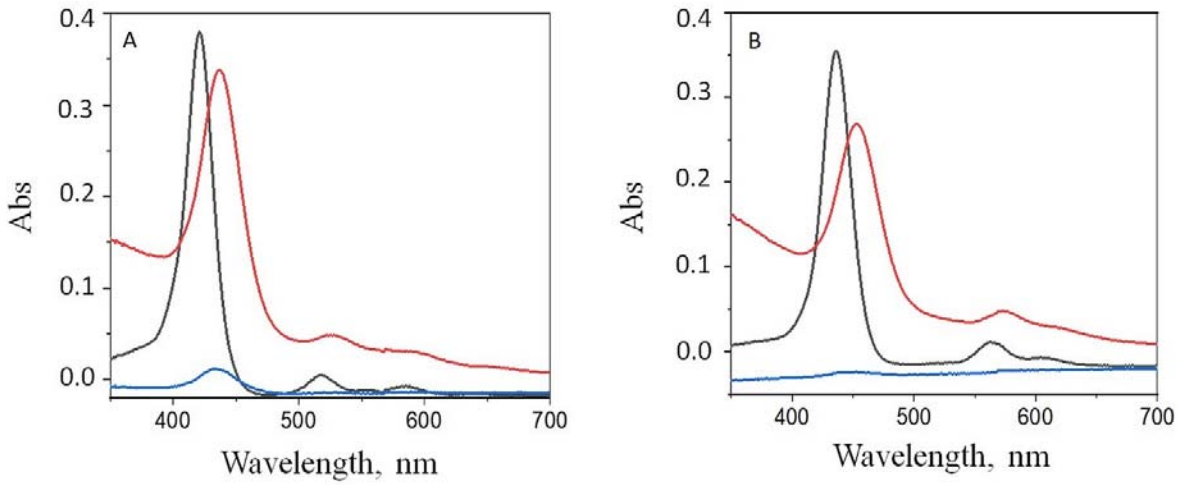

Figure 4 UV-vis absorption spectra of A) free TMPyP (black), TMPyP after adding GO (red) and the supernatant after centrifugation (blue), B) free ZnTMPyP (black), ZnTMPyP after adding GO (red) and the supernatant after centrifugation (blue).

To estimate the maximum amount of porphyrin that can be adsorbed onto the GO surface, reverse titration measurements were conducted (Figure 5). To a solution of GO with a fixed concentration, different amounts of porphyrin solutions were added. After exceeding the concentration of TMPyP and ZnTMPyP above 6.42 μM absorbance of the Soret band attributed to free porphyrin started to be visible. This amount of TMPyP or ZnTMPyP was taken as the maximum amount of the porphyrin that can be adsorbed on the 0.039 mg or 0.015 mg of GO, respectively. These values were recalculated into 1 mg of GO.

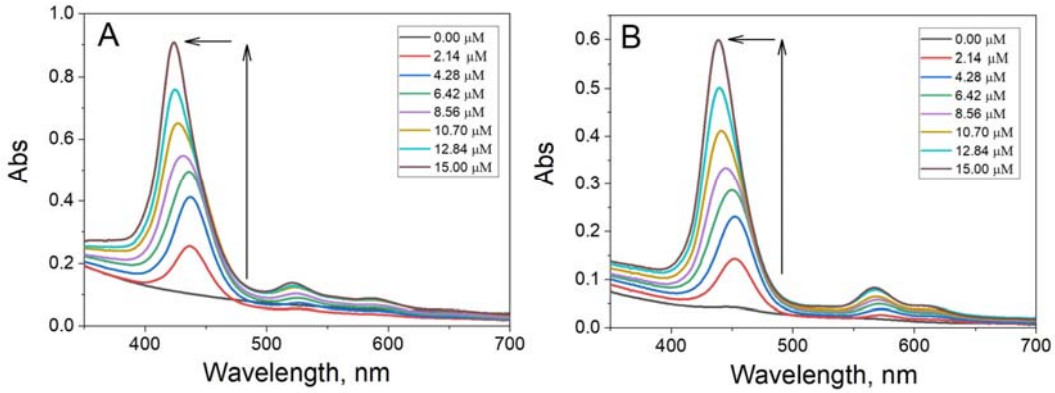

Figure 5 A) Absorption spectra obtained during gradual addition of TMPyP solution (0 – 15 μM) to 3mL aqueous suspension of GO (0.013 mg mL^{-1}) B) Absorption spectra obtained during gradual addition of ZnTMPyP (0 – 15 μM) to 3mL aqueous suspension of GO 0.005 mg mL^{-1}.

Based on the obtained UV-vis spectra it was estimated that the maximum amount of TMPyP in TMPyP-GO is less than 5% (% w/w) whereas nearly 0.11 mg of ZnTMPyP can be adsorbed onto 1 mg of GO surface (9.9%, % w/w).

Emission measurements

Emission spectroscopy was used to probe electronic interactions of the excited state of the porphyrin molecules with a GO sheet. As previously discussed, the absorption spectra of TMPyP and ZnTMPyP changes upon introduction of GO to the solution. To ensure the same absorbance at the excitation wavelength during quenching emission experiments, that is essential for quantitative analysis,[50] solutions were excited at the isosbestic points (Table S1). Addition of the GO aqueous suspension to aqueous solutions of porphyrins led to a decrease in the porphyrin fluorescence intensity (Figure 6). To compare the efficiency of TMPyP and ZnTMPyP

fluorescence quenching by GO, the emission spectra presented in Figure 6 were carried out with the amount of GO added (1.9×10^{-4} mg mL^{-1}) kept constant. Thus, it is clear that the fluorescence of TMPyP is quenched less efficiently by GO than the fluorescence of ZnTMPyP. The quenching efficiency for the GO concentration 1.9×10^{-4} mg mL^{-1} was calculated to be 50% and 17% for ZnTMPyP and TMPyP, respectively.

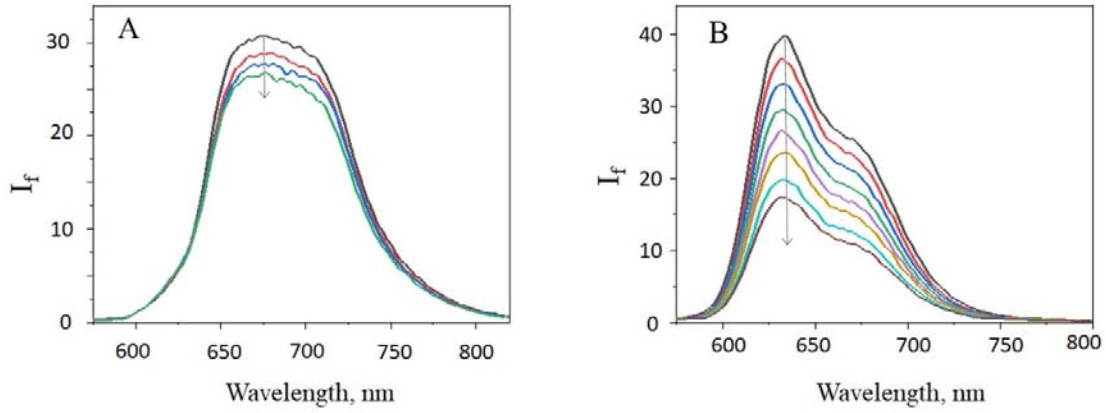

Figure 6 A) Quenching of the fluorescence of 0.50 µM TMPyP in H_2O measured upon adding of GO ($0 - 1.9 \times 10^{-4}$ mg mL^{-1}) excitation at 434 nm, B) Quenching of the fluorescence of 0.16 µM ZnTMPyP in H_2O measured upon adding of GO ($0 - 1.9 \times 10^{-4}$ mg mL^{-1}) excitation at 447 nm.

To quench 50% of the TMPyP emission, a GO concentration of 4.2×10^{-4} mg mL^{-1} was required (Figure S12). Based on the results of the steady-state emission experiment, it can be stated that the emissions of both porphyrins were quenched very efficiently by GO in comparison to other porphyrin/graphene-based materials. For example, Masih *et al.*[51] reported that for ZnTMPyP the quenching efficiency was 50% at a graphene carboxylate concentration of 5.7×10^{-3} mg mL^{-1}, and Wojcik *et al.* measured a 50% emission quenching efficiency of TMPyP at an RGO concentration of 0.8×10^{-3} mg mL^{-1}.[42] In general, it is observed that an electrostatic interaction between the cationic porphyrin and the negatively charged graphene material enhances quenching of the

porphyrin emission,[29,42,51] in comparison to the neutral porphyrin where the interaction with the graphene-based material is attributed mainly to π-π stacking interactions.[21,47,51,52]

The higher quenching efficiency of ZnTMPyP indicated that the interaction of GO with ZnTMPyP is stronger in comparison to TMPyP. The exact quenching mechanism cannot be determined reliably based solely on steady-state emission data. Mechanisms that should be taken into account for the explanation of the observed decrease of porphyrin (TMPyP and ZnTMPyP) emissions in the presence of GO are dynamic and static quenching of the free porphyrin by GO. The distinction between these two mechanisms was addressed by applying the time-correlated single photon counting technique. In the case of dynamic quenching, the additional deactivation pathway, i.e. quenching of the excited state by GO, should shortens the observed lifetime of the fluorescence. In contrast, in static quenching, the lifetime does not change since porphyrin and GO form a non-emissive complex in the ground state, and hence, remaining free porphyrin in solution is able to emit after excitation and will have normal excited state properties. Those mechanisms were tested by measuring the emission lifetimes of TMPyP and ZnTMPyP in the presence of GO (Figure 7). From the decay profile of TMPyP and ZnTMPyP without GO, the emission lifetimes were found to be c.a. 5.7 ns and 1.3 ns, respectively. With the gradual addition of GO, the kinetics traces of the excited state remained unchanged in both cases. One would normally have expected a shortening of the singlet excited state of unbound porphyrin if the quenching were the result of a dynamic process induced by GO. There might also be the chance to see the appearance of a second decay associated with any fluorescence of the nanohybrid. Neither of these decays was detected during the time correlated single photon counting experiment. This observation eliminates the possibility of dynamic quenching by GO as the mechanism for the observed decrease of the porphyrin emission intensity upon GO addition. Our comprehensive analysis of the emission

quenching (steady-state and time-resolved) indicates that it was entirely due to static quenching of the porphyrin by GO.[29]

Moreover, TMPyP-GO and ZnTMPyP-GO have different ground state absorption spectra in comparison to the free porphyrins, thus any emission from the composite material would be expected to be shifted to longer wavelengths relative to free TMPyP and ZnTMPyP. However, upon addition of the GO suspension to either TMPyP or ZnTMPyP solution, no detectable changes in the shapes of the emission spectra were noticed (Figure S13). In addition, as presented in Figure S14, the fluorescence excitation spectrum recorded for TMPyP and ZnTMPyP solutions after the addition of GO overlapped perfectly with the absorption spectrum of the unbound porphyrins.

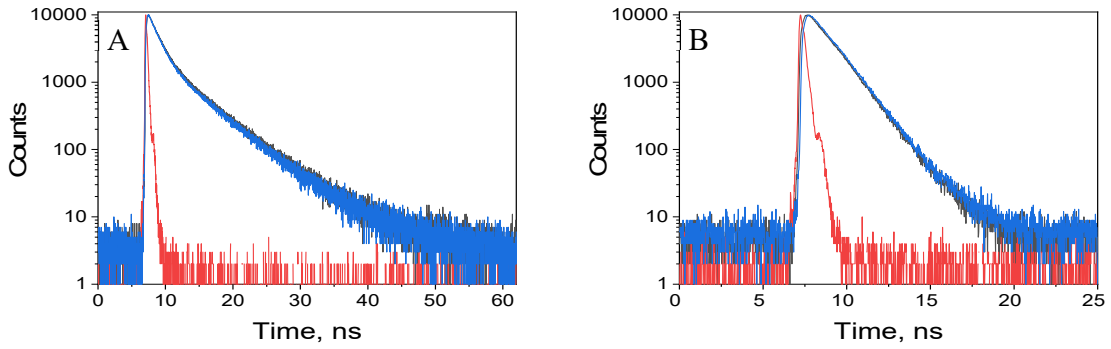

Figure 7 Decay of A) TMPyP fluorescence recorded in the absence (black) and presence (blue) of GO, prompt (red); λ_{ex} = 440 nm, λ_{em} = 650 nm, B) ZnTMPyP fluorescence recorded in the absence (black) and presence (blue) of GO, prompt (red); λ_{ex} = 440 nm, λ_{em} = 693 nm.

In summary, based on the data presented above, it can be stated that both hybrid materials, TMPyP-GO and ZnTMPyP-GO, are not emissive materials and that the free porphyrins are the only emissive species present in the solutions.

No measurable emission from the complexes TMPyP-GO and ZnTMPyP-GO indicated that another very rapid process was responsible for the quenching of the singlet excited state ($^1S^*$) of the porphyrins. To probe the possibility of an electron transfer (ET) process, the free energy of ET from the $^1S^*$ of the porphyrin to GO was calculated by applying the Rehm–Weller equation.[53,54] Based on the data summarized in Table 1 and conduction band edge of GO equal to -0.55 V *vs.* NHE,[55] the free energy of the ET from the $^1S^*$ of porphyrin molecules and GO were estimated (Table1). The negative value of the free energy of ET for ZnTMPyP (-0.11eV) and the slightly positive for TMPyP (0.02 eV) indicates that photoinduced electron transfer could possibly take place in both cases.

Table 1 Zero−zero transitions of the singlet excited state of TMPyP and ZnTMPyP, their oxidation potentials and the driving force of the electron-transfer reaction values.

Porphyrin	$E_{0\text{-}0}$ (eV)	E_{ox} (V vs. NHE)	E^*_{ox} (V vs. NHE)	G_{ET} (eV)
TMPyP	2.07	1.54[56]	-0.53	0.02
ZnTMPyP	2.08	1.42[56]	-0.66	-0.11

Femtosecond Transient Absorption Spectroscopy

Ultrafast transient absorption experiments were conducted in order to monitor the influence of the GO on the deactivation pathways of $^1S^*$ of the porphyrins. The transient spectra recorded immediately after a 422 nm laser pulse excitation of free ZnTMPyP is characterized by an intense absorption around 475-525 nm, which is typical for the $^1S^*$ of the porphyrins.[42,57] In addition, bleaching of the Q-bands was observed at the wavelengths that match the ground state absorption spectra (Figure 8A). The lifetime of $^1S^*$ of ZnTMPyP determined from the kinetic profile at 590 nm was equal to 1.45 ns. This value coincides well with the value determined independently in the

TCSPC experiment (Figure S15). The disappearance of the absorption from the $^1S^*$ of ZnTMPyP during 3 ns (the maximum delay in the experimental setup) was accompanied by only small changes in the spectrum. The growth of a weak signal around 675 nm and the presence of an isosbestic point at 700 nm were observed. Those changes in the absorption spectra of $^1S^*$ with time can be attributed to the formation of the triplet excited state. It is known that the singlet excited state of ZnTMPyP undergoes intersystem crossing to form the triplet excited state, but, due to the large similarity of both transient absorption spectra, the spectral evolution observed in femtosecond transient absorption spectroscopy is small.[51,58]

An analogous transient absorption (TA) experiment was performed after adding GO to the ZnTMPyP (Figure 8B). It is clear that the TA spectra of ZnTMPyP-GO (Figure 8B) look differently in comparison to free ZnTMyP (Figure 8A). For a proper interpretation of the data it is important to correct the spectra for the transient absorbance of the GO itself (Figure S13).[59,60]

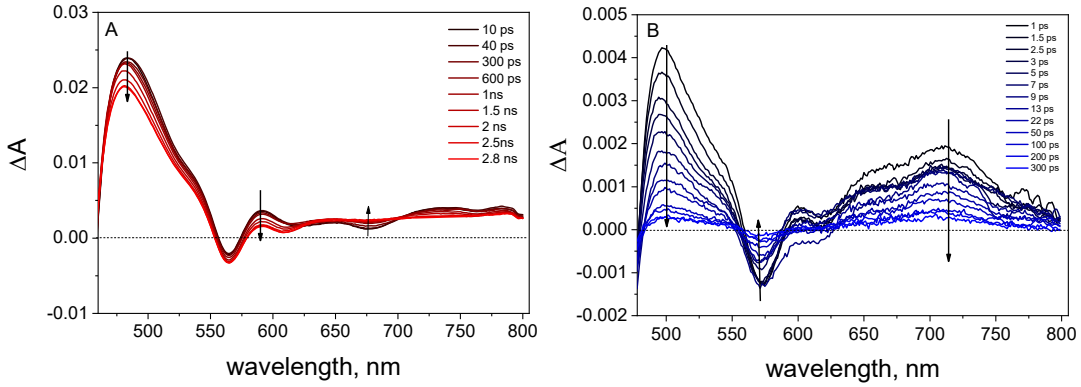

Figure 8 Transient absorption spectra obtained at different time delays for A) ZnTMPyP (8 μM) and B) ZnTMPyP-GO (ZnTMPyP concentration 8.0 μM, GO concentration 0.01 mg mL^{-1}) in water following the 437 nm laser excitation for A) and 453 nm laser excitation for B). Transient absorption spectra in B) was corrected for the contribution from GO itself.

If left uncorrected the observed transient absorption spectra of the porphyrin-GO system can be falsely interpreted in terms of electron transfer processes (see uncorrected spectra in Figure S17 for comparison). The transient absorption spectra recorded just after the excitation is different in comparison to the analogous spectra recorded for free ZnTMPyP. As presented in Figure 8B, formation of an additional band in the region of 650-800 nm was detected. This band has been assigned to the porphyrin radical cation $ZnTMPyP^{+\bullet}$ by comparison to the spectra for the $ZnTMPyP^{+\bullet}$ described previously in the literature.[51,59] The observation of the $ZnTMPyP^{+\bullet}$ gives clear evidence for photoinduced ET from porphyrin to GO.

Comparison of the time profiles registered at 710 nm for free ZnTMPyP and for ZnTMPyP after addition of GO reveals significant difference in decay dynamics (Figure 9).

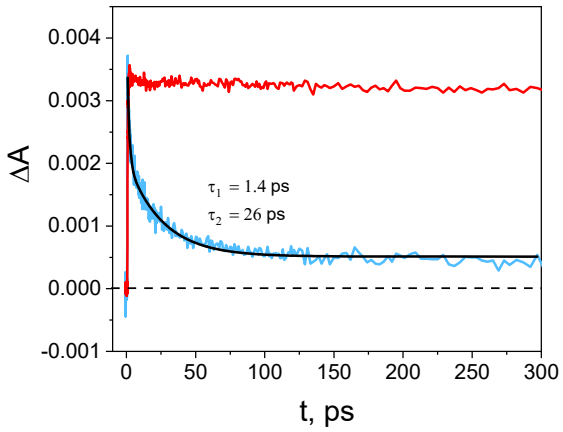

Figure 9 Absorption time profiles at 710 nm measured for the ZnTMPyP (red) and ZnTMPyP-GO (blue) following the 437 nm and 453 nm laser excitation, respectively (black line shows the three exponential decay fit).

In comparison to free ZnTMyP, the time profiles for the ZnTMyP bound to GO sheet exhibits very fast decay that could be well fitted to a two exponential decay function. The time constants obtained from the fit to the 710 nm decay profile attributed to the $ZnTMPyP^{+\bullet}$ are 1.4 ps and 26 ps. It was found previously that back electron transfer within the ion pair of the $ZnTMPyP^{+\bullet}$ and graphene carboxylate occurs with the time constant of 20.18 ps, which is in the same range as the value obtained it this work.[42] Aly *et al.* and Larowska *et al.* reported two time constants ranging from several to tens of picoseconds for the decay of the TMAP radical cation formed in the presence of graphene carboxylate and graphene oxide, respectively.[29,48] The authors proposed that the decay of the porphyrin radical cation with two time constants originates from various geometries of the porphyrin molecules in the nanohybrid material. It is worth noting that the radical cation of ZnTMPyP in our system was observed immediately after the excitation (temporal resolution of the setup 300 fs), pointing to a very fast electron transfer from ZnTMPyP to GO. Such fast photoinduced ET can occur only when the donor and acceptor are already in very close connection before excitation. Disappearance of the signal from $ZnTMPyP^{+\bullet}$ can be explained by back electron transfer. This is confirmed by a comparison of the bleach recovery at 575 nm which follows the same kinetics as the kinetic decay at 710 nm. Interestingly, in all of the decay profiles, a residual signal (offset) of about 14% was present. This signal is explained by a fraction of the ZnTMPyP radical cation which did not undergo back electron transfer during our probed time window of 3 ns. Varying geometries of the ZnTMPyP-GO nanoassemblies may influence the rate constant of the back electron transfer.

The transient absorption spectra measured immediately after the 422 nm laser pulse excitation of TMPyP exhibited an intense signal around 450-500 nm and four signals from bleach, whose position matched with the Q-band of TMPyP measured for the ground state absorption spectra (*ca.*

518, 555, 584 and 643 nm, see Figure 10A and Figure S18). The transient absorption kinetics were found to be biexponential. The transient spectra showed a fast component of about 16 ps that can be assigned to either an excited state conformational change or a vibrational cooling path via releasing excess energy from solute to solvent.[61–63] The slow component with a lifetime of 3.8 ns (value with the error since the whole time window of the experiment is 2.8 ns) is attributed to the decay of $^1S^*$. Upon addition of GO to TMPyP, the transient absorption spectra after correction for the GO absorption (Figure S19) showed almost no difference in comparison to the spectra recorded for the unbound TMPyP (see Figure 10B). Only the position of the bleach signal changed from 520 nm to 528 nm in agreement with the ground state absorption spectra. No appreciable increase in the absorption above 600 nm was observed, which would have indicated the presence of the TMPyP radical cation.[42,57] Formation of the TMPyP radical cation has been reported in the presence of graphene carboxylate, however the authors did not mention whether the transient absorption spectra were corrected for the GO transient absorption.[57]

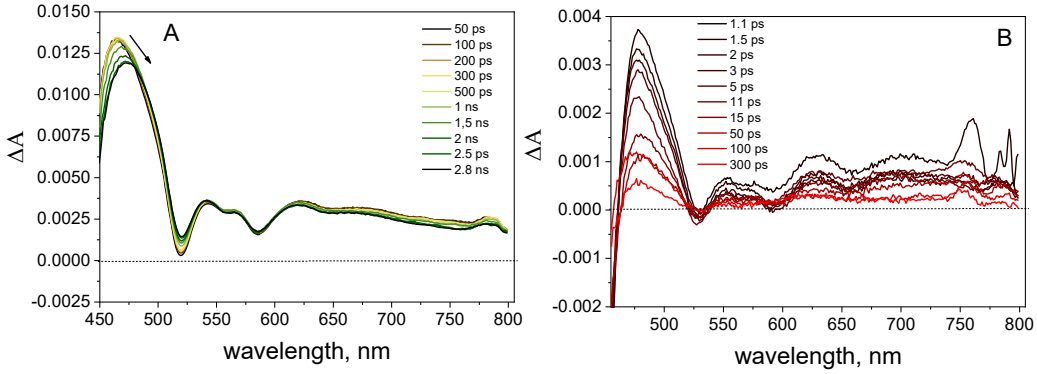

Figure 10 Transient absorption spectra measured at different time delays for A) TMPyP (5 μM) and B) TMPyP-GO (TMPyP concentration 5.0 μM, GO concentration 0.01 mg mL^{-1}) in water following the 422 nm laser excitation for A) and 437 nm laser excitation for B). Transient absorption spectra in B) was corrected for the contribution from GO itself.

Comparison of the time profiles measured for free TMPyP and TMPyP bound to the GO surface are depicted in Figure 11. The transient absorption at 480 nm for $^1S^*$ of free TMPyP remained almost constant during 150 ps after excitation whereas the time profile for the TMPyP-GO exhibited fast decay. When TMPyP is adsorbed on the GO surface, its $^1S^*$ lifetime was reduced remarkably, and its decay was biexponential with lifetimes of 1.5 ps and 25 ps. It demonstrates a strong influence of the GO on the properties of TMPyP in its photoexcited state. The possible explanation for the fast decay of the $^1S^*$ of TMPyP attached to the GO sheet is an electron transfer. The lack of any detection of the radical cation of the porphyrin, that would constitute unambiguous evidence for any electron transfer, can be explained by similar rates of electron transfer and back electron transfer.

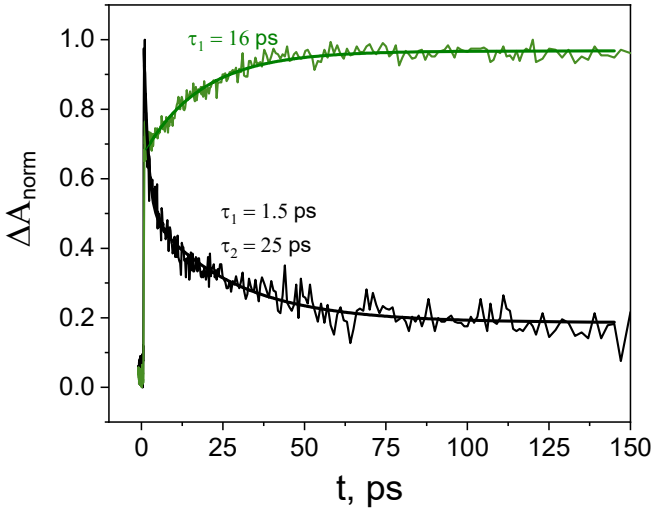

Figure 11 Absorption time profiles at 480 nm measured for TMPyP (green) and TMPyP-GO (black) following the 422 nm and 437 nm laser excitation, respectively.

2.3 Photoelectrical response measurement

Experimental support for the photoinduced charge separation mechanism comes from complementary photocurrent measurements. Figure 12 shows photoelectrical response of the SnO_2/FTO electrode covered with GO, TMPyP-GO, and ZnTMPyP-GO films, respectively. The irradiation was switched on and off in alternating 30s periods in order to measure the light and dark current responses. From the Figure 12 it can be seen that the photocurrent response of GO film was insignificant.

However, an obvious photocurrent response for the electrode covered with TMPyP-GO and ZnTMPyP-GO films was observed under similar experimental conditions. This increase in photocurrent provides evidence for the photoinduced charge transfer in the studied materials. The produced photocurrent was almost constant or decreased by 15% in the three on/off irradiation cycles for TMPyP-GO and ZnTMPyP-GO films, respectively.

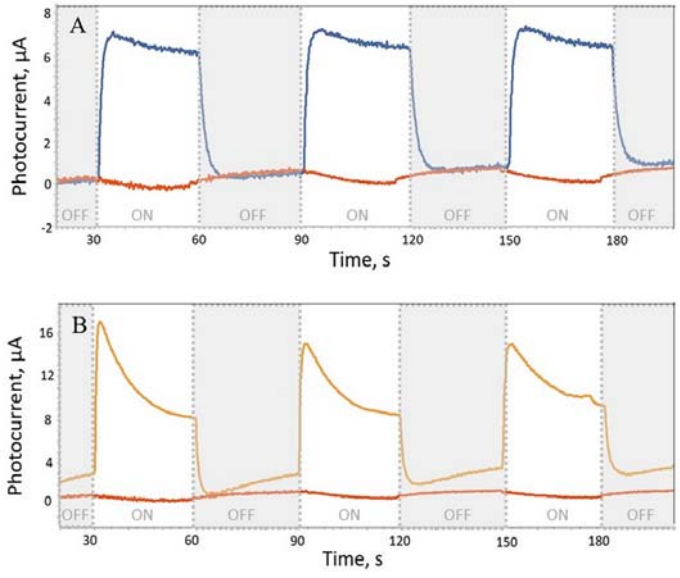

Figure 12 Transient photocurrent in time for A) TMPyP-GO and B) ZnTMPyP-GO under white light illumination (electrolyte: 0.1 M LiI in acetonitrile). In both A an B, the red line shows the photocurrent generated by GO.

The photocurrent generated by the ZnTMPyP-GO sample was about 2 times larger than that generated by the TMPyP-GO sample. The higher photocurrent response for ZnTMPyP-GO sample might be attributed to more efficient electron-hole separations, and hence, it can explain the higher photocatalytic activity of the ZnTMPyP-GO material (*vide infra*).

Photocatalytic activity of porphyrin-GO composites

The photocatalytic performance for degrading RhB was examined under visible light irradiation for three materials: GO, TMPyP-GO and ZnTMPyP-GO. Prior to illumination, the suspensions of RhB and the photocatalysts were continuously stirred overnight to reach an adsorption–desorption equilibrium. Afterwards, the samples were irradiated for 2h under visible light with constant stirring. Decreases of the RhB concentration in the samples were determined spectrophotochemically by measuring changes in the absorbance at 554 nm, the maximum absorbance for RhB (Figure 13). As shown in Figure 13, for the control experiment without the addition of any photocatalyst, a very small degradation of RhB molecules (3% after 2 h) could be observed. All of the photocatalyst samples were catalytically active for the decomposing of RhB using visible light irradiation. In order to quantitatively compare the photocatalytic performance of the hybrid materials, the absorbance of the porphyrins in both composite materials was kept constant in order to ensure the absorption of the same amount of photons by the samples. Interestingly, the activity of the as-prepared ZnTMPyP-GO nanoassembly was the highest, resulting in 19% RhB decomposition after 2 h (value corrected for the photodegradation of RhB itself). The activity of the pure GO sample was significantly lower than that of the hybrid materials (3.7% RhB decomposition). The free porphyrins without GO did not show any photocatalytic activity towards RhB degradation (Figure S20). Lack of any photocatalytic activity of the

porphyrins themself can be attributed to their instability under light irradiation and to a significant decrease in light absorption upon their decomposition (Figure S21). TMPyP and ZnTMyP were tested as photocatalysts as monomers, however, it was proven recently that it is the self-assembly of porphyrins which leads to catalytic performance, and that photocatalytic performance depends on the morphology of the porphyrin nanostructures.[16,64]

Interestingly, it was observed that the adsorption of the TMPyP and ZnTMPyP onto the GO surface significantly improved the photostability of the porphyrins (Figure S21). After 2 h of irradiation, decomposition of the porphyrins in the porphyrin-GO hybrids was negligible.

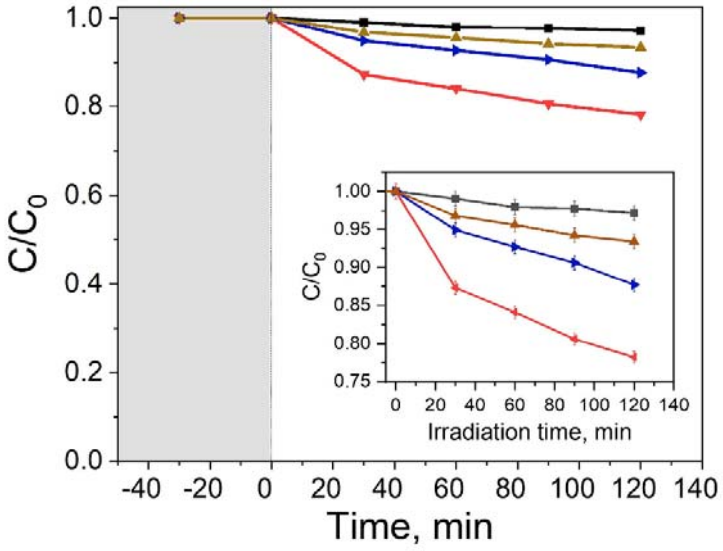

Figure 13 RhB photodegradation under visible irradiation (λ > 400 nm): control (black, ■), GO (brown, ▲), TMPyP-GO composite (blue, ►) and ZnTMPyP-GO composite (red, ▼).

The experimental data were plotted as a function of ln(C/C0) *vs.* time in order to obtain the rate constants for the photocatalytic reaction. The degradation of RhB could be described with a

pseudo-first order kinetics model (Figure S22), and the rate constants of the reaction were found to be *ca.* 1.9×10^{-3} min^{-1} and 1.0×10^{-3} min^{-1} for ZnTMPyP-GO and TMPyP-GO, respectively. The photocatalytic degradation of RhB with graphene nanoplates supported by (4-carboxyphenyl)porphyrin (TCCP) aggregates was found to occur with a rate constant of *ca.* 7.3×10^{-3} min^{-1}.[25] The rate constant for RhB degradation was further increased to 9.4×10^{-3} min^{-1} by applying ternary nanostructure graphene@TiO_2@TCCP.[31] It was shown that supramolecular ZnTPyP porphyrin based nanofibers display photocatalytic activity toward RhB degardation.[16] The performance of the ZnTPyP supramolecular assemblies was enhanced by functionalizing with GO sheet.[21] The rate constant of 2.6×10^{-2} min^{-1} was reported for ZnTPyP supramolecular nanostructures assembled on the GO sheet.[21] One has to be aware that any comparison between the reported systems needs to be done with caution since the photocatalytic activity of these systems depends not only on the catalytic activity of the photocatalyst itself, but also on the experimental conditions such as the concentrations of both RhB and the photocatalyst, or the power of the light source.

The UV-vis absorption spectra of our systems show a band shift from 554 nm, the maximum absorption of RhB, to 530 nm (Figure S20). As reported earlier, this effect indicates that photodegradation occurs *via* N-deethylation.[65–71] It was found that photodegradation of RhB was negligible if the experiment was performed under an argon atmosphere indicating that the presence of oxygen is essential. Generally, it is known that when a photocatalyst is irradiated by light, various reactive oxygen species (ROS) which can degrade the pollutants. The work function of graphene oxide was estimated to be *ca.* 4.2 eV.[55,72] Taking into account reported electrochemical data for ZnTMPyP,[56] the LUMO (–4.14 eV) and HOMO (–6.17 eV) energy levels were calculated and depicted in Scheme 1.[72] By analyzing those data and our steady-state and time-resolved

spectroscopic measurements, a possible mechanism for the enhanced activity of the porphyrin-GO composite towards RhB degradation can be summarized as follows (Scheme 1): the porphyrin electrons can be photoexcited from the S_0 to the S_1^* LUMO level and then transferred to the GO sheet leading to the formation of electron–hole pairs. The reaction between the photogenerated holes on the surface of TMPyP and ZnTMPyP and H_2O or OH^- results in the formation of hydroxyl radical $OH^{\bullet}$, which can oxidize RhB to degradable products. On the other hand, the photogenerated electron on the graphene oxide sheet can react with oxygen molecules dissolved in H_2O and produce the oxygen superoxide anion $O_2^{\bullet-}$. Singlet oxygen ($^1O_2$) is usually formed in the energy transfer process from the triplet excited state of the molecule to the oxygen triplet ground state. In the case of our porphyrin-GO materials, based on our femtosecond transient absorption spectroscopy, the formation of the triplet excited state of the porphyrin is fully suppressed. Very fast deactivation of the singlet excited state of porphyrin *via* electron transfer to GO excludes intersystem crossing processes and thus, population of the triplet state of the porphyrin. As no porphyrin in the triplet excited state is formed, it is concluded that singlet oxygen does not participate in RhB degradation. In summary, the formation of reactive oxygen species ($OH^{\bullet}$ and $O_2^{\bullet-}$) leads to degradation of RhB in water. The efficiency of the generation of ROS is expected to be higher for the ZnTMPyP-GO system, due to formation of longer-lived charge separated states.

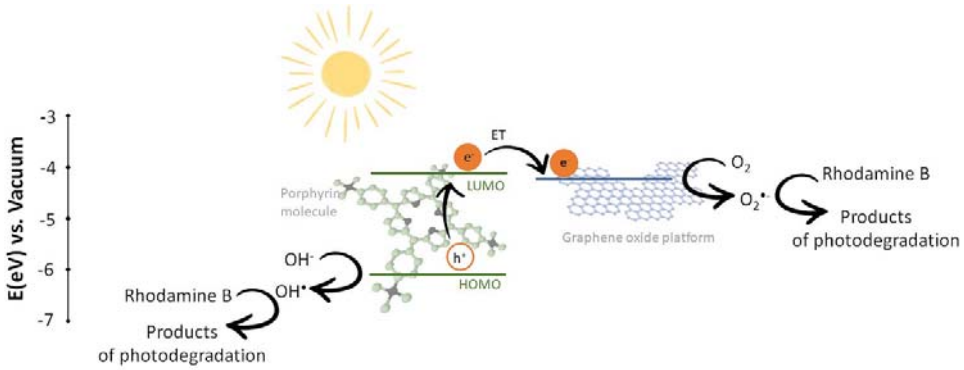

Scheme 1 Proposed mechanism for RhB photodegradation by porphyrin-GO nanohybrids (porphyrin = TMPyP, ZnTMPyP).

Conclusion

Two nanohybrids TMPyP-GO and ZnTMPyP-GO were prepared by non-covalent attachment of the cationic porphyrins to GO surfaces and described using various spectroscopic methods with the aim of generating a photocatalyst active for RhB degradation. The nanohybrids are comprised of water-soluble porphyrins bearing peripheral positive charges as the electron donor, and noncovalently functionalized GO as the electron acceptor. Spectroscopic measurements demonstrated that both porphyrins can be assembled onto a GO surface *via* non-covalent interactions and that the new material can be prepared and isolated by combining the solutions of porphyrin and GO followed by centrifugation. Our comprehensive steady-state absorption and emission data analysis allowed us to conclude that metalation of TMPyP with Zn(II) increased the affinity of the porphyrin towards the graphene oxide surface. Photocurrent measurements and femtosecond transient absorption spectroscopy provided evidence for electron transfer occurring in the hybrid materials.

Both hybrid materials, TMPyP-GO and ZnTMPyP-GO, demonstrated higher photocatalytic activity towards RhB degradation as compared to GO, however ZnTMPyP-GO exhibited a much more efficient performance. Our data indicates that the presence of Zn in the core of the porphyrin can promote charge separation in the ZnTMPyP-GO composites. The higher degradation rate seen with ZnTMPyP-GO as compared to the TMPyP-GO assemblies highlights the beneficial role of Zn(II)-metalation of the porphyrin ring.

ASSOCIATED CONTENT

Supporting Information

Synthesis, ^{1}H NMR, and MALDI spectra of 5,10,15,20-tetrakis(4-pyridyl)porphyrin, TMPyP and ZnTMPyP. AFM image of GO and depth profile of GO, TMPyP-GO and ZnTMPyP-GO, normalized UV-vis spectra of free TMPyP and ZnTMPyP adsorbed on GO, Normalized fluorescence spectra of TMPyP and ZnTMPyP in the absence and presence of GO, normalized fluorescence excitation spectrum of the mixture of TMPyP with GO and ZnTMPyP and GO, transient absorption spectra of GO, transient absorption spectra for ZnTMPyP-GO without correction for the transient absorbance of the GO itself, transient absorption spectra registered at early time delays for TMPyP, UV-Vis spectra of TMPyP and ZnTMPyP aqueous solution under 2 h Vis-irradiation in the absence and presence of GO, UV-Vis spectra of RhB solution with addition of ZnTMPyP-GO during irradiation.

AUTHOR INFORMATION

Corresponding Author

***Email: alewand@amu.edu.pl**

Funding Sources

This research was financially supported by the National Science Centre (project no. 2015/19/D/ST5/00682), Science Foundation Ireland (SFI, IvP 13/IA/1894) and grant no. POWR.03.02.00-00-I026/16 co-financed by the European Union through the European Social Fund under the Operational Program Knowledge Education Development. The project has received funding from the European Union's Horizon 2020 research and innovation program under the FET Open grant agreement no. 828779.

Conflicts of interest

There are no conflicts to declare.

ACKNOWLEDGMENT

This research was financially supported by the National Science Centre (project no. 2015/19/D/ST5/00682), Science Foundation Ireland (SFI, IvP 13/IA/1894) and grant no. POWR.03.02.00-00-I026/16 co-financed by the European Union through the European Social Fund under the Operational Program Knowledge Education Development. The project has received funding from the European Union's Horizon 2020 research and innovation program under the FET Open grant agreement no. 828779. DL thanks Professor Ian Carmichael, the director of the Radiation Laboratory, University of Notre Dame for financial support during her stay in the Rad Lab and Dr Artur Ciesielski from Université de Strasbourg, CNRS, ISIS for the access to the equipment during her stay in ISIS.

References

(1) Richardson, S. D.; Willson, C. S.; Rusch, K. A. Use of Rhodamine Water Tracer in the Marshland Upwelling System. *Ground Water* **2004**, *42*, 678–688.

(2) Nestmann, E. R.; Douglas, G. R.; Matula, T. I.; Grant, C. E.; Kowbel, D. J. Mutagenic Activity of Rhodamine Dyes and Their Impurities as Detected by Mutation Induction in Salmonella and DNA Damage in Chinese Hamster Ovary Cells. *Cancer Res.* **1979**, *39*, 4412–4417.

(3) Dire, D. J.; Wilkinson, J. A. Acute Exposure to Rhodamine. **1987**, *5*, 603–607.

(4) Soltani, T.; Entezari, M. H. Chemical Photolysis and Photocatalysis of Methylene Blue by Ferrite Bismuth Nanoparticles under Sunlight Irradiation. *J. Mol. Catal. A, Chem.* **2013**, *377*, 197–203.

(5) Crini, G. Non-Conventional Low-Cost Adsorbents for Dye Removal : A Review. *Bioresour. Technol.* **2006**, *97*, 1061–1085.

(6) Viswanathan, B. Photocatalytic Degradation of Dyes: An Overview. *Curr. Catal.* **2017**, *7* , 99–121.

(7) Legrini, O.; Oliveros, E.; Braun, A. M. Photochemical Processes for Water Treatment. *Chem. Rev.* **1993**, *93*, 671–698.

(8) Ajmal, A.; Majeed, I.; Malik, R. N.; Iqbal, M.; Nadeem, M. A.; Hussain, I.; Yousuf, S.; Zeshan; Mustafa, G.; Zafar, M. I.; Nadeem, M. A. Photocatalytic Degradation of Textile Dyes on Cu_2O-CuO/TiO_2 Anatase Powders. *J. Environ. Chem. Eng.* **2016**, *4*, 2138–2146.

(9) Shirzadi, A.; Nezamzadeh-Ejhieh, A. Enhanced Photocatalytic Activity of Supported CuO-ZnO Semiconductors towards the Photodegradation of Mefenamic Acid Aqueous Solution as a Semi Real Sample. *J. Mol. Chem. Catal. A, Chem*. **2016,** *411*, 222-229.

(10) Bora Akin, M.; Oner, M. Photodegradation of Methylene Blue with Sphere-like ZnO Particles Prepared via Aqueous Solution. *Ceram. Int.* **2013**, *39*, 9759–9762.

(11) Li, D.; Ohashi, N.; Hishita, S.; Kolodiazhnyi, T.; Haneda, H. Origin of Visible-Light-Driven Photocatalysis: A Comparative Study on N/F-Doped and N-F-Codoped TiO_2 Powders by Means of Experimental Characterizations and Theoretical Calculations. *J. Solid State Chem.* **2005**, *178*, 3293–3302.

(12) Wangab, Y.; Ma, X.; Li, H.; Liu, B.; Li, H.; Yin, S.; Sato, T. Recent Advances in Visible-Light Driven Photocatalysis in *Advanced Catalytic Matererials - Photocatalysis and Other Currernt Trends*, Luis Enrique Norena and Jin-An Wang, InTechOpen, **2016**.

(13) Tsao, J.; Lewis, N.; Crabtree, G. Solar FAQs. *US Dep. Energy* **2006**, 1–24.

(14) Kielmann, M.; Prior, C.; Senge, M. O. Porphyrins in Troubled Times: A Spotlight on Porphyrins and Their Metal Complexes for Explosives Testing and CBRN Defense. *New J. Chem.* **2018**, *42*, 7529–7550.

(15) De Napoli, M.; Nardis, S.; Paolesse, R.; Vicente, M. G. H.; Lauceri, R.; Purrello, R. Hierarchical Porphyrin Self-Assembly in Aqueous Solution. *J. Am. Chem. Soc.* **2004**, *126*, 5934–5935.

(16) Guo, P.; Chen, P.; Ma, W.; Liu, M. Morphology-Dependent Supramolecular Photocatalytic Performance of Porphyrin Nanoassemblies: From Molecule to Artificial Supramolecular Nanoantenna. *J. Mater. Chem.* **2012**, *22*, 20243–20249.

(17) Kamat, P. V. Graphene-Based Nanoassemblies for Energy Conversion. *J. Phys. Chem. Lett.* **2011**, *2*, 242–251.

(18) Bai, S.; Shen, X. Graphene-Inorganic Nanocomposites. *RSC Adv.* **2012**, *2*, 64–98.

(19) Luo, B.; Liu, S.; Zhi, L. Chemical Approaches toward Graphene-Based Nanomaterials and Their Applications in Energy-Related Areas. *Small* **2012**, *8*, 630–646.

(20) MacHado, B. F.; Serp, P. Graphene-Based Materials for Catalysis. *Catal. Sci. Technol.* **2012**, *2*, 54–75.

(21) Guo, P.; Chen, P.; Liu, M. One-Dimensional Porphyrin Nanoassemblies Assisted via Graphene Oxide: Sheetlike Functional Surfactant and Enhanced Photocatalytic Behaviors. *ACS Appl. Mater. Interfaces* **2013**, *5*, 5336–5345.

(22) Chen, Y.; Huang, Z. H.; Yue, M.; Kang, F. Integrating Porphyrin Nanoparticles into a 2D Graphene Matrix for Free-Standing Nanohybrid Films with Enhanced Visible-Light Photocatalytic Activity. *Nanoscale* **2014**, *6*, 978–985.

(23) Ussia, M.; Bruno, E.; Spina, E.; Vitalini, D.; Pellegrino, G.; Ruffino, F.; Privitera, V.; Carroccio, S. C. Freestanding Photocatalytic Materials Based on 3D Graphene and Polyporphyrins. *Sci. Rep.* **2018**, *8*, 1–12.

(24) Ussia, M.; Urso, M.; Miritello, M.; Bruno, E.; Curcuruto, G.; Vitalini, D.; Condorelli, G. G.; Cantarella, M.; Privitera, V.; Carroccio, S. C. Hybrid Nickel-Free Graphene/Porphyrin Rings for Photodegradation of Emerging Pollutants in Water. *RSC Adv.* **2019**, *9*, 30182–30194.

(25) La, D. D.; Rananaware, A.; Salimimarand, M.; Bhosale, S. V. Well–Dispersed Assembled Porphyrin Nanorods on Graphene for the Enhanced Photocatalytic Performance. *ChemistrySelect* **2016**, *1*, 4430–4434.

(26) El-Shafai, N.; El-Khouly, M. E.; El-Kemary, M.; Ramadan, M. S.; Masoud, M. S. Self-Assembly of Porphyrin on Graphene Oxide in Aqueous Medium: Fabrication, Characterization, and Photocatalytic Studies. *Photochem. Photobiol. Sci.* **2019**, *18*, 2071–2079.

(27) Lu, Q.; Zhang, Y.; Liu, S. Graphene Quantum Dots Enhanced Photocatalytic Activity of

Zinc Porphyrin toward the Degradation of Methylene Blue under Visible-Light Irradiation. *J. Mater. Chem. A* **2015**, *3*, 8552–8558.

(28) Kiessling, D.; Costa, R. D.; Katsukis, G.; Malig, J.; Lodermeyer, F.; Feihl, S.; Roth, A.; Wibmer, L.; Kehrer, M.; Volland, M.; Wagner, P.; Wallace, G. G.; Officer, D. L.; Guldi, D. M. Novel Nanographene/Porphyrin Hybrids – Preparation, Characterization, and Application in Solar Energy Conversion Schemes. *Chem. Sci.* **2013**, *4*, 3085–3098.

(29) Larowska, D.; Wojcik, A.; Mazurkiewicz-Pawlicka, M.; Malolepszy, A.; Stobiński, L.; Marciniak, B.; Lewandowska-Andralojc, A. Cationic Porphyrin-Graphene Oxide Hybrid: Donor-Acceptor Composite for Efficient Photoinduced Electron Transfer. *ChemPhysChem* **2019**, *20*, 1054-1066.

(30) Ussia, M.; Ruffino, F.; Bruno, E.; Spina, E.; Conticello, I.; Privitera, V.; Carroccio, S. C. The Role of Solvent on the Formulation of Graphene/Polyporphyrin Hybrid Material versus Photocatalytic Activity. *Polym. Bull.* **2020**, *77*, 2073–2087.

(31) La, D. D.; Bhosale, S. V.; Jones, L. A.; Revaprasadu, N.; Bhosale, S. V. Fabrication of a Graphene@TiO_2@Porphyrin Hybrid Material and Its Photocatalytic Properties under Simulated Sunlight Irradiation. *ChemistrySelect* **2017**, *2*, 3329–3333.

(32) La, D.; Hangarge, R.; V. Bhosale, S.; Ninh, H.; Jones, L.; Bhosale, S. Arginine-Mediated Self-Assembly of Porphyrin on Graphene: A Photocatalyst for Degradation of Dyes. *Appl. Sci.* **2017**, 7, 643.

(33) Bera, R.; Mandal, S.; Mondal, B.; Jana, B.; Nayak, S. K.; Patra, A. Graphene-Porphyrin Nanorod Composites for Solar Light Harvesting. *ACS Sustain. Chem. Eng.* **2016**, *4*, 1562–

1568.

(34) Yao, M.; Meng, Y.; Mao, X.; Ning, X.; Zhang, Z.; Shan, D.; Chen, J.; Lu, X. New Insight into Enhanced Photocatalytic Activity of Morphology-Dependent TCPP-AGG/RGO/Pt Composites. *Electrochim. Acta* **2018**, *282*, 575–581.

(35) Phuangburee, T.; Solonenko, D.; Plainpan, N.; Thamyongkit, P.; Zahn, D. R. T.; Unarunotai, S.; Tuntulani, T.; Leeladee, P. Surface Modification of Graphene Oxide via Noncovalent Functionalization with Porphyrins for Selective Photocatalytic Oxidation of Alcohols . *New J. Chem.* **2020**, 44, 8264-8272.

(36) Zhang, L.; Qin, L.; Kang, S. Z.; Li, G. D.; Li, X. Graphene/Pyridylporphyrin Hybrids Interfacially Linked with Rare Earth Ions for Enhanced Photocatalytic Hydrogen Evolution. *ACS Sustain. Chem. Eng.* **2019**, *7*, 8358–8366.

(37) Wang, J.; Zhong, Y.; Wang, L.; Zhang, N.; Cao, R.; Bian, K.; Alarid, L.; Haddad, R. E.; Bai, F.; Fan, H. Morphology-Controlled Synthesis and Metalation of Porphyrin Nanoparticles with Enhanced Photocatalytic Performance. *Nano Lett.* **2016**, *16*, 6523–6528.

(38) Gacka E.: Burdzinski G.: Marciniak B.: Kubas A.: Lewandowska-Andrałojć A. Interaction of Light with a Non-Covalent Zinc Porphyrin–Graphene Oxide Nanohybrid. *Phys. Chem. Chem. Phys.* **2020**, *19*..

(39) Yuan, Y. J.; Chen, D.; Zhong, J.; Yang, L. X.; Wang, J. J.; Yu, Z. T.; Zou, Z. G. Construction of a Noble-Metal-Free Photocatalytic H2 Evolution System Using MoS2/Reduced Graphene Oxide Catalyst and Zinc Porphyrin Photosensitizer. *J. Phys. Chem. C* **2017**, *121*, 24452–24462...

(40) Gouterman, M.; Wagnière, G. H.; Snyder, L. C. Spectra of Porphyrins. Part II. Four Orbital Model. *J. Mol. Spectrosc.* **1963**, *11*, 108–127.

(41) Gouterman, M. Spectra of Porphyrins. *J. Mol. Spectrosc.* **1961**, *6*, 138–163.

(42) Wojcik, A.; Kamat, P. V. Reduced Graphene Oxide and Porphyrin. An Interactive Affair in 2-D. *ACS Nano* **2010**, *4*, 6697–6706.

(43) Marsh, D. F.; Mink, L. M. Microscale Synthesis and Electronic Absorption Spectroscopy of Tetraphenylporphyrin H_2(TPP) and Metalloporphyrins Zn^{II}(TPP) and Ni^{II}(TPP). *J. Chem. Educ.* **1996**, *73*, 1188–1190.

(44) Kano, K.; Minamizono, H.; Kitae, T.; Negi, S. Self-Aggregation of Cationic Porphyrins in Water. Can π-π Stacking Interaction Overcome Electrostatic Repulsive Force? *J. Phys. Chem. A* **1997**, *101*, 6118–6124.

(45) Becerril, H. A.; Mao, J.; Liu, Z.; Stoltenberg, R. M.; Bao, Z.; Chen, Y. Evaluation of Solution-Processed Reduced Graphene Oxide Films as Transparent Conductors. *ACS Nano* **2008**, *2*, 463–470.

(46) Xu, Y.; Zhao, L.; Bai, H.; Hong, W.; Li, C.; Shi, G. Chemically Covnerted Graphene Indcuded Molecular Flattenin of 5,10,15,20-Tetrakis(1-Methyl-4-Pyridino)Porphyrin and Its Application. *J. Am. Chem. Soc.* **2009**, *131*, 13490–13497.

(47) Gacka, E.; Wojcik, A.; Mazurkiewicz-Pawlicka, M.; Malolepszy, A.; Stobiński, L.; Kubas, A.; Hug, G. L.; Marciniak, B.; Lewandowska-Andralojc, A. Noncovalent Porphyrin-Graphene Oxide Nanohybrids: The pH-Dependent Behavior. *J. Phys. Chem. C* **2019**, *123*, 3368–3380.

(48) Chernia, Z.; Gill, D. Flattening of TMPyP Adsorbed on Laponite. Evidence in Observed and Calculated UV-Vis Spectra. *Langmuir* **1999**, *15*, 1625–1633.

(49) Orth, E. S.; Ferreira, J. G. L.; Fonsaca, J. E. S.; Blaskievicz, S. F.; Domingues, S. H.; Dasgupta, A.; Terrones, M.; Zarbin, A. J. G. PKa Determination of Graphene-like Materials: Validating Chemical Functionalization. *J. Colloid Interface Sci.* **2016**, *467*, 239–244.

(50) Lewandowska-Andralojc, A.; Marciniak, B. Five Major Sins in Fluorescence Spectroscopy of Light-Harvesting Hybrid Materials. *ACS Energy Lett.* **2019**, *4*, 1898–1901.

(51) Masih, D.; Aly, S. M.; Usman, A.; Alarousu, E.; Mohammed, O. F. Real-Time Observation of Ultrafast Electron Injection at Graphene-Zn Porphyrin Interfaces. *Phys. Chem. Chem. Phys.* **2015**, *17*, 9015–9019.

(52) Ye, T. X.; Ye, S. L.; Chen, D. M.; Chen, Q. A.; Qiu, B.; Chen, X. Spectroscopic Characterization of Tetracationic Porphyrins and Their Noncovalent Functionalization with Graphene. *Spectrochim. Acta - Part A Mol. Biomol. Spectrosc.* **2012**, *86*, 467–471.

(53) Rehm, D.; Weller, A. Kinetik Und Mechanismus Der Elektronübertragung Bei Der Fluoreszenzlöschung in Acetonitril. *Ber. Bunsenges. Phys. Chem.* **1969**, *73*, 834.

(54) Rehm, D.; Weller, A. Bindungszustand Und Fluoreszenzspektren von Hetero-Excimeren. *Isr. J. Chem.* **1970**, *8*, 259.

(55) Yeh, T. F.; Chan, F. F.; Hsieh, C. Te; Teng, H. Graphite Oxide with Different Oxygenated Levels for Hydrogen and Oxygen Production from Water under Illumination: The Band Positions of Graphite Oxide. *J. Phys. Chem. C* **2011**, *115*, 22587–22597.

(56) Kalyanasundaram, K.; Neumann-Spallart, M. Photophysical and Redox Properties of Water-Soluble Porphyrins in Aqueous Media. *J. Phys. Chem.* **1982**, *86*, 5163–5169.

(57) Aly, S. M.; Parida, M. R.; Alarousu, E.; Mohammed, O. F. Ultrafast Electron Injection at the Cationic Porphyrin-Graphene Interface Assisted by Molecular Flattening. *Chem. Commun.* **2014**, *50*, 10452–10455.

(58) Barbosa Neto, N. M.; Correa, D. S.; De Boni, L.; Parra, G. G.; Misoguti, L.; Mendonça, C. R.; Borissevitch, I. E.; Zílio, S. C.; Gonçalves, P. J. Excited States Absorption Spectra of Porphyrins - Solvent Effects. *Chem. Phys. Lett.* **2013**, *587*, 118–123.

(59) Kaniyankandy, S.; Achary, S. N.; Rawalekar, S.; Ghosh, H. N. Ultrafast Relaxation Dynamics in Graphene Oxide: Evidence of Electron Trapping. *J. Phys. Chem. C* **2011**, *115*, 19110–19116.

(60) Wen, X.; Yu, P.; Toh, Y. R.; Lee, Y. C.; Huang, K. Y.; Huang, S.; Shrestha, S.; Conibeer, G.; Tang, J. Ultrafast Electron Transfer in the Nanocomposite of the Graphene Oxide-Au Nanocluster with Graphene Oxide as a Donor. *J. Mater. Chem. C* **2014**, *2*, 3826–3834.

(61) Laermer, F.; Elsaesser, T.; Kaiser, W. Ultrashort Vibronic and Thermal Relaxation of Dye Molecules after Femtosecond Ultraviolet Excitation. *Chem. Phys. Lett.* **1989**, *156*, 381–386.

(62) Retsek, J. L.; Gentemann, S.; Medforth, C. J.; Smith, K. M.; Chirvony, V. S.; Fajer, J.; Holten, D. Photoinduced Evolution on the Conformational Landscape of Nonplanar Dodecaphenylporphyrin: Picosecond Relaxation Dynamics in The $^{1}(\pi,\Pi^{*})$ Excited State. *J. Phys. Chem. B* **2000**, *104*, 6690–6693.

(63) Enescu, M.; Steenkeste, K.; Tfibel, F.; Fontaine-Aupart, M. P. Femtosecond Relaxation

Processes from Upper Excited States of Tetrakis(N-Methyl-4-Pyridyl)Porphyrins Studied by Transient Absorption Spectroscopy. *Phys. Chem. Chem. Phys.* **2002**, *4*, 6092–6099.

(64) Mandal, S.; Nayak, S. K.; Mallampalli, S.; Patra, A. Surfactant Assisted Porphyrin Based Hierarchical Nano / Micro Assemblies and Their Efficient Photocatalytic Behaviour Surfactant Assisted Porphyrin Based Hierarchical Nano / Micro Assemblies and Their Efficient Photocatalytic Behaviour. *CS Appl. Mater. Interfaces* **2014**, 6, 130-136.

(65) Wang, Q.; Li, J.; Bai, Y.; Lu, X.; Ding, Y.; Yin, S.; Huang, H.; Ma, H.; Wang, F.; Su, B. Photodegradation of Textile Dye Rhodamine B over a Novel Biopolymer–Metal Complex Wool-Pd/CdS Photocatalysts under Visible Light Irradiation. *J. Photochem. Photobiol. B Biol.* **2013**, *126*, 47–54.

(66) Chen, F.; Zhao, J.; Hidaka, H. Highly Selective Deethylation of Rhodamine B: Adsorption and Photooxidation Pathways of the Dye on the TiO_2/SiO_2 Composite Photocatalyst. *Int. J. Photoenergy* **2003**, *5*, 209–217.

(67) Liu, G.; Li, X.; Zhao, J.; Hidaka, H.; Serpone, N. Photooxidation Pathway of Sulforhodamine-B. Dependence on the Adsorption Mode on TiO_2 Exposed to Visible Light Radiation. *Environ. Sci. Technol.* **2000**, *34*, 3982–3990.

(68) Pica, M.; Calzuola, S.; Donnadio, A.; Gentili, P. L.; Nocchetti, M.; Casciola, M. De-Ethy Lation and Cleavage of Rhodamine b by a Zirconium Phosphate/Silver Bromide Composite Photocatalyst. *Catalysts* **2019**, *9*.

(69) Morín, M. E. Z.; Torres-Martínez, L.; Sanchez-Martínez, D.; Gómez-Solís, C. Photocatalytic Performance of Titanates with Formula $MTiO_3$ (M= Fe, Ni, and Co)

Synthesized by Solvo-Combustion Method. *Mater. Res.* **2017**, *20*, 1322–1331.

(70) Yu, K.; Yang, S.; He, H.; Sun, C.; Gu, C.; Ju, Y. Visible Light-Driven Photocatalytic Degradation of Rhodamine B over $NaBiO_3$: Pathways and Mechanism. *J. Phys. Chem. A* **2009**, *113*, 10024–10032.

(71) Wang, P.; Cheng, M.; Zhang, Z. On Different Photodecomposition Behaviors of Rhodamine B on Laponite and Montmorillonite Clay under Visible Light Irradiation. *J. Saudi Chem. Soc.* **2014**, *18*, 308–316.

(72) Cardona, C. M.; Li, W.; Kaifer, A. E.; Stockdale, D.; Bazan, G. C. Electrochemical Considerations for Determining Absolute Frontier Orbital Energy Levels of Conjugated Polymers for Solar Cell Applications. *Adv. Mater.* **2011**, *23*, 2367–2371.

TOC Graphic